Magneto-optical properties of Co/Ir superstructures on Ir(111)

C. Etz,[1,*] A. Vernes,[2] and P. Weinberger[1,3]

[1]*Max-Planck-Institut für Mikrostrukturphysik, Weinberg 2, DE-06120 Halle (Saale), Germany*
[2]*Austrian Center of Competence for Tribology, Viktor-Kaplan-Strasse 2, AT-2700 Wiener Neustadt, Austria*
[3]*Center for Computational Nanoscience, Seilerstätte 10/22, AT-1010 Vienna, Austria*

The fully relativistic spin-polarized screened Korringa-Kohn-Rostoker method is used to evaluate the electronic and magnetic structure as well as the optical conductivity of $(Co_mIr_m)_n$ superstructures on Ir(111). By mapping the microscopic optical conductivity tensor onto the macroscopic permittivity tensor and by using the so-called 2×2 matrix technique the surface reflectivity matrices for these systems are then calculated, from which in turn the Kerr rotation and ellipticity angles can be determined. It is found (i) that when varying at a given value of m the number of repetitions n, these angles are linearly proportional to the total magnetic moment, and (ii) that at a frequency of about 3.8 eV the Kerr rotation angles have the largest value, the corresponding maximum being mainly caused by the Ir spacer layers. The optical properties of the free surface of Ir(111), which is considered to check the applied theoretical schemes, turn out to be in good agreement with existing experimental data.

PACS number(s): 75.70.−i, 78.20.−e, 78.68.+m

I. INTRODUCTION

When John Kerr published his observations of the reflection of light from the pole of a (horse-shoe) magnet,[1–3] he probably did not envisage that about 130 years later one would still speak of a "polar" and a "longitudinal"[2] magneto-optical effect. Even his statement that "...magneto-optics.... must be all included ultimately under one physical theory"[2] remained valid up to now. John Kerr probably never thought that "his" effect would become one of the most commonly used experimental tools in (nano)magnetism.

In the last 30 years, Kerr measurements were first used in the field of nanomagnetism, for example, to trace reorientation transitions in magnetic thin-film systems[4] and then applied to magnetic superstructures on nonmagnetic substrates such as (Co/Cu) on Cu.[5] In particular, superstructures of the type $(Co_mPt_p)_n$ on Pt(111)[6–9] raised considerable interest because of possible applications in the field of magneto-optical storage media. Less studies were performed on (Co/Ir) superstructures on Ir(111).[10,11] In the wide majority of present-day applications, the Kerr effect is mainly used as a "finger-print" method to map the properties of magnetic surfaces.

In the following, a theoretical study of the magneto-optical properties of $(Co_mIr_m)_n$ superstructures on Ir(111) substrate is presented. Completely in line with John Kerr's demand of "one physical theory," it turned out that the Kerr rotation and ellipticity angles of such superstructures offer interesting features and possible future applications. In particular, for example, it will be shown that the Ir spacer layers are of a crucial importance for the size of the Kerr rotation angles. It is also the aim of this paper to stress the importance of considering the macroscopic nature of magneto-optical measurements.

II. THEORETICAL APPROACH

A. Permittivities

In a system characterized by two-dimensional translational symmetry referring to scattering regions disjoint in configurational space, the macroscopic permittivity tensor can be written to a very good approximation in terms of a sum over layer-resolved permittivity tensors,[14–16]

$$\epsilon(\omega; N) = \frac{1}{N} \sum_{p=1}^{N} \epsilon^p(\omega), \quad (1)$$

$$\epsilon^p(\omega) = \sum_{q=1}^{N} \epsilon^{pq}(\omega), \quad (2)$$

where N is the total number of atomic layers considered. The $\epsilon^{pq}(\omega)$ in Eq. (2) results from a mapping of corresponding elements of the microscopic optical conductivity $\sigma^{pq}(\omega)$,[13,16]

$$\epsilon^{pq}(\omega) = \mathrm{I}\delta_{pq} + \frac{4\pi i}{\omega} \sigma^{pq}(\omega), \quad (3)$$

from which in turn the real and imaginary parts of the dielectric tensor can be easily identified:

$$\mathrm{Re}\epsilon(\omega; N) = \mathrm{I} - \frac{4\pi}{\omega} \left[\frac{1}{N} \sum_{p=1}^{N} \mathrm{Im}\sigma^p(\omega) \right],$$

$$\mathrm{Im}\epsilon(\omega; N) = \frac{4\pi}{\omega} \left[\frac{1}{N} \sum_{p=1}^{N} \mathrm{Re}\sigma^p(\omega) \right], \quad \text{for } \omega \in \mathbb{R}$$

where I is the 3×3 unit matrix.

The actual form of $\epsilon(\omega; N)$ reflects of course the underlying (two-dimensional) rotational symmetry of the system under investigation and the type of spectroscopy performed (polar or longitudinal geometry).

1. Substrate

Since paramagnetic Ir(111) bulk is of fcc type ($a_0 = 7.2545$ a.u.), in terms of three-dimensional cyclic boundary conditions the layer-dependent permittivity tensors can be written as[14]

$$\epsilon^p(\omega) = \begin{pmatrix} \epsilon_{xx}^p(\omega) & 0 & 0 \\ 0 & \epsilon_{yy}^p(\omega) & 0 \\ 0 & 0 & \epsilon_{zz}^p(\omega) \end{pmatrix}, \quad (4)$$

$$\epsilon_{xx}^p(\omega) = \epsilon_{yy}^p(\omega), \quad (5)$$

where x and y refer to the in-plane coordinates and z is parallel to the surface normal. If, however, only two-dimensional translational symmetry applies, as is the case of an Ir(111) free surface, then the following conditions have to be fulfilled numerically:

$$\left| \epsilon_{zz}^{N+m}(\omega) - \epsilon_{zz}^{N}(\omega) \right| < \delta, \quad m \in \mathbb{N}, \tag{6}$$

$$\lim_{m \to M} \epsilon_{zz}^{N+m}(\omega) = \epsilon_{zz}(\omega), \tag{7}$$

where in principle δ is an infinitesimally small number and M a sufficiently large positive integer. Equations (6) and (7) imply that only well inside the Ir(111) substrate full cubic symmetry is restored.

2. Co/Ir superstructures

Considering in polar geometry Co/Ir superstructures on Ir(111), $\epsilon^p(\omega)$ can be written as[14]

$$\epsilon^p(\omega) = \begin{pmatrix} \epsilon_{xx}^p(\omega) & \epsilon_{xy}^p(\omega) & 0 \\ -\epsilon_{xy}^p(\omega) & \epsilon_{xx}^p(\omega) & 0 \\ 0 & 0 & \epsilon_{zz}^p(\omega) \end{pmatrix}, \tag{8}$$

and again the condition (6) has to be met.

Quite obviously, in calculating the magneto-optical properties of $(Co_m Ir_m)_n/Ir(111)$ the following gradual change in the form of $\epsilon^p(\omega)$ has to be taken into account, namely, from the bulk-like interior of the substrate to the vacuum region,

$$\underbrace{\begin{pmatrix} \epsilon_{xx} & 0 & 0 \\ 0 & \epsilon_{xx} & 0 \\ 0 & 0 & \epsilon_{xx} \end{pmatrix}}_{\text{bulk}} \rightarrow \underbrace{\begin{pmatrix} \epsilon_{xx}^p(\omega) & \epsilon_{xy}^p(\omega) & 0 \\ -\epsilon_{xy}^p(\omega) & \epsilon_{xx}^p(\omega) & 0 \\ 0 & 0 & \epsilon_{zz}^p(\omega) \end{pmatrix}}_{\text{substrate near surface \& superstructures}}$$

$$\rightarrow \underbrace{\begin{pmatrix} 1 & 0 & 0 \\ 0 & 1 & 0 \\ 0 & 0 & 1 \end{pmatrix}}_{\text{vacuum}}. \tag{9}$$

B. Kerr rotation and ellipticity angles

By starting, as sketched in relation (9), well inside the substrate and solving sequentially in each layer the Fresnel, Helmholtz, and curl Maxwell equations, the surface reflectivity matrix $\mathbf{R}$,

$$\begin{pmatrix} E_{\text{vac},x}^{(r)} \\ E_{\text{vac},y}^{(r)} \end{pmatrix} = \mathbf{R} \begin{pmatrix} E_{\text{vac},x}^{(i)} \\ E_{\text{vac},y}^{(i)} \end{pmatrix}, \tag{10}$$

can be obtained in terms of the so-called 2×2 matrix technique that takes into account all reflections and interferences within the layered system.[12,14–16]

Matrix $\mathbf{R}$ relates (in the vacuum) the magnitudes of the components, $E_{\text{vac},\nu}^{(i)}$, where $\nu = x$ and y, of the electric field corresponding to the incident (i) light beam to those of the reflected (r) light beam, $E_{\text{vac},\nu}^{(r)}$. In the case of polar geometry (and an fcc parent lattice), $\mathbf{R}$ has the form

$$\mathbf{R} = \begin{pmatrix} R_{xx} & R_{xy} \\ -R_{xy} & R_{xx} \end{pmatrix}. \tag{11}$$

For further details see Refs. 14 and 16. Expressed in spherical coordinates, the complex reflectivity of the right- (+) and left-handed (−) circularly polarized light is then given by

$$R_\pm = R_{xx} \mp i R_{xy} = \frac{E_\pm^{(r)}}{E^{(i)}}$$

$$= |R_\pm| e^{i \Delta_\pm}, \tag{12}$$

where $E_\pm^{(r)}$ is the complex amplitude of the reflected right- and left-handed circularly polarized light and $E^{(i)}$ that of the incident light. Variable $\Delta_\pm$ is the phase of the complex reflectivity $R_\pm$. The Kerr rotation θ_K and ellipticity ϵ_K angles are finally defined by[14]

$$\theta_K = -\frac{1}{2}(\Delta_+ - \Delta_-), \tag{13}$$

$$\epsilon_K = -\frac{|r_+| - |r_-|}{|r_+| + |r_-|}, \tag{14}$$

or, in terms of a complex Kerr angle Φ_K, as

$$\Phi_K = \theta_K + i \epsilon_K.$$

It is useful at this stage to recall that the Kerr rotation and ellipticity angles are clearly macroscopic quantities.
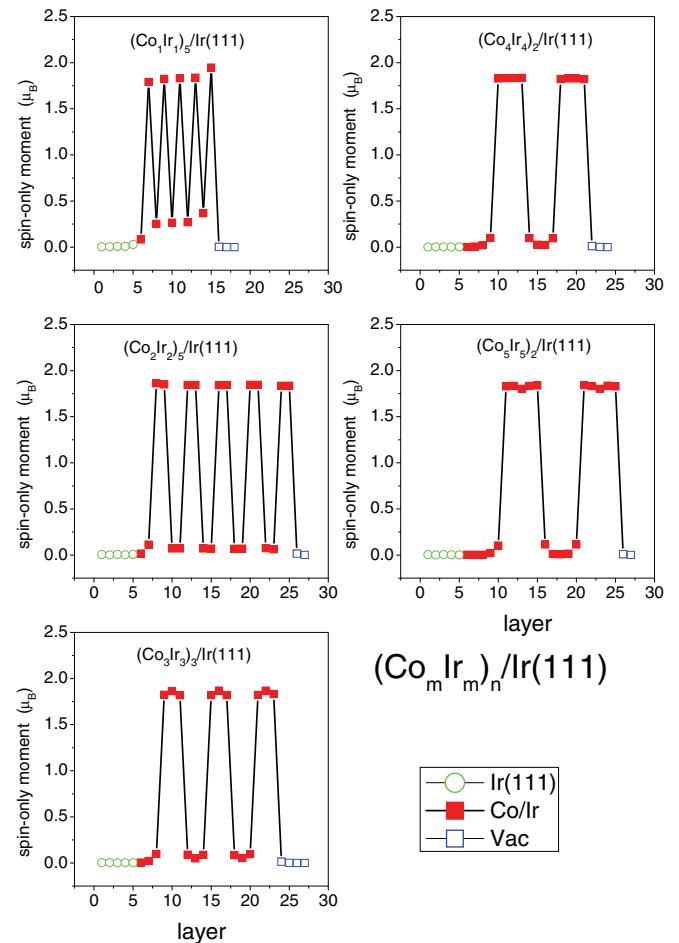

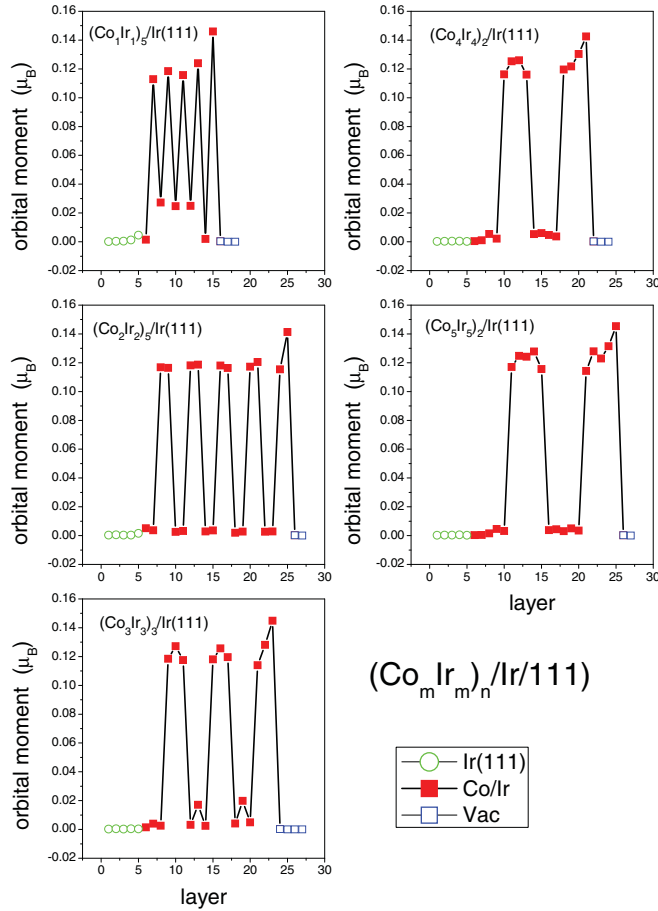FIG. 1. (Color online) Layer-resolved spin-only magnetic moments in $(Co_m Ir_m)_n/Ir(111)$.

FIG. 2. (Color online) Layer-resolved orbital magnetic moments in $(Co_m Ir_m)_n/Ir(111)$.

III. COMPUTATIONAL DETAILS

All self-consistent *ab initio* electronic-structure calculations were performed for a uniform direction of the magnetization pointing along the surface normal in terms of the spin-polarized (fully) relativistic screened Korringa-Kohn-Rostoker method for layered systems, within density functional theory (DFT).[16,17] The $\sigma^{pq}(\omega)$ in Eq. (3) are calculated in terms of Luttinger's formula[13,18] using again the spin-polarized relativistic screened Korringa–Kohn–Rostoker method, contour-integration techniques,[13] the Konrod quadrature, and the cumulative special-points method for the occurring Brillouin-zone integrals.[19] It should be noted that Luttinger's formalism uses a vector-potential description of the electric field and has several advantages over the well-known Kubo formula;[20] both, the absorptive and dissipative parts of the conductivity tensor are included without using the Kramers-Kronig relations, and so are all inter- and intra-band contributions, avoiding thus a phenomenological Drude term in order to mimic the latter contributions. In all calculations, a maximum angular quantum number $l = 2$ was considered[17] and the exchange-correlation functional parametrization of Ref. [21] and the atomic sphere approximation (ASA) are applied.

IV. RESULTS

Since it is not possible to show for each combination of m and n in $(Co_m Ir_m)_n/Ir(111)$ all obtained results, in the following, particular values of m and n are chosen (m denotes the number of Co and Ir atomic layers, while n gives the number of repetitions). This is, in particular, the case for the permittivities for the real and the imaginary parts of ϵ as functions of m, n, and ω ought to be displayed. The only exception will be the Kerr rotation and ellipticity angles, since they are directly observable and represent the main goal of this paper.

A. Magnetic moments

As examples, the spin-only and orbital magnetic moments for $(Co_1 Ir_1)_5$, $(Co_2 Ir_2)_5$, $(Co_3 Ir_3)_3$, $(Co_4 Ir_4)_2$, and $(Co_5 Ir_5)_2$ on Ir(111) are displayed in Figs. 1 and 2. It is perhaps surprising to see that the spin and orbital magnetic moments of Co vary very little in these systems, only the orbital moment of the top
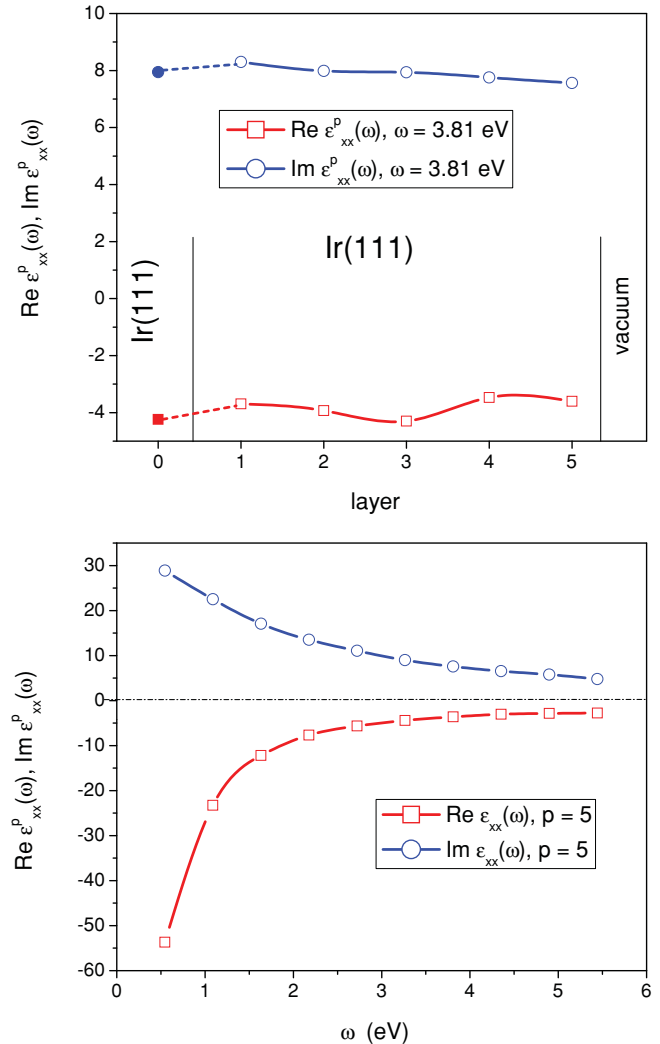

FIG. 3. (Color online) Permittivities for a free surface of Ir(111). Top: layer-resolved permittivities for $\omega = 3.81$ eV (open symbols), full symbols represent the Ir bulk values; bottom: frequency dependence of the permittivity in the top Ir layer.

Co layer differs significantly from all interior Co layers. Less surprising are the rather small moments of the Ir layers in the superstructures, since it is quite well established by now that Ir is much less polarizable than Pt, see, for example, Ref. 23. If m_p denotes the total magnetic moment in layer p and $\langle m_{Co} \rangle$ an averaged Co moment (per layer), then Figs. 1 and 2 suggest that the total magnetic moment M of a particular system can, to a very good approximation, be replaced by the sum over all moments in Co layers:

$$M = \sum_{p=1}^{N} m_p \sim mn \langle m_{Co} \rangle . \tag{15}$$

B. Permittivities

1. Substrate

As already mentioned, it is important to consider enough bulk substrate layers[22] in the procedure sketched in Eq. (9). For matters of checking the applied numerical procedures,
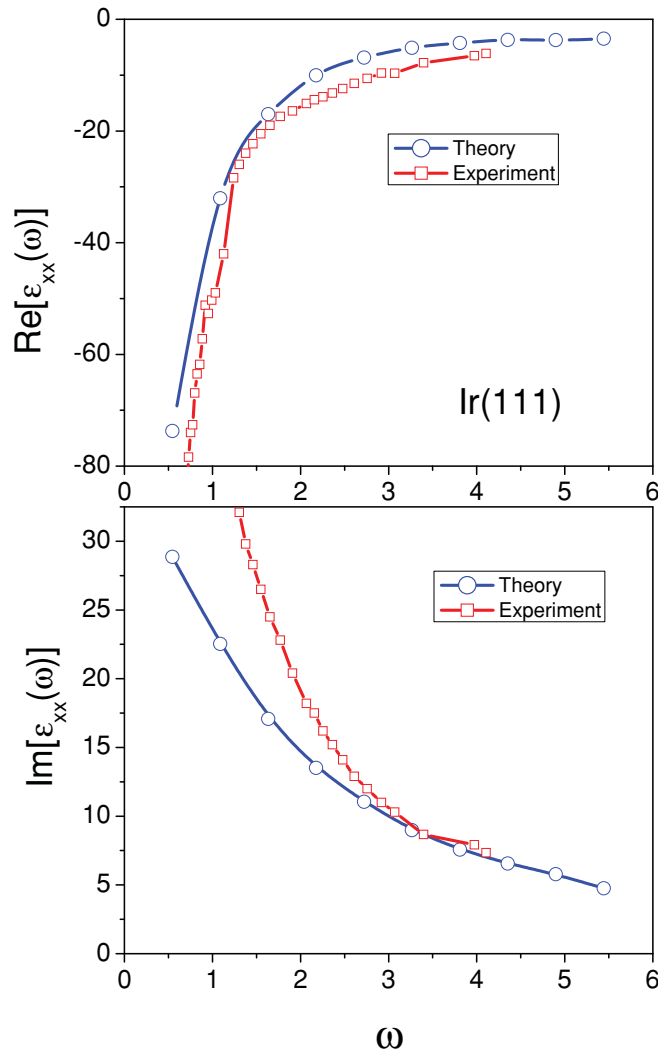

FIG. 4. (Color online) Comparison of the real and imaginary parts of bulk permittivity ϵ_{xx} for Ir(111) between calculated and experimental data at 77 K.[29]

first, a free surface of Ir(111) was considered, since at least in this case experimental data are available to which the present calculations can be compared with. In the upper part of Fig. 3, the real and the imaginary parts of the layer-resolved permittivities $\varepsilon_{xx}^{p}(\omega)$ at a particular frequency, namely $\omega = 3.81$ eV, are displayed versus the layer index p. As can be seen, for a fixed frequency, Re$[\varepsilon_{xx}^{p}(\omega)]$ and Im$[\varepsilon_{xx}^{p}(\omega)]$ vary only little when viewed from the surface, marked as "vacuum," toward the interior of Ir(111). Inspecting the variation of a chosen layer-dependent permittivity, see the top Ir layer, $p = 5$, in the lower part of this figure, with respect to the frequency of the incident radiation, a strong dependency can be observed; at a frequency of about 5.5 eV both the real and the imaginary parts of this particular layer-resolved permittivity are only about a tenth of the value registered at $\omega \sim 0.5$ eV.

This strong frequency dependence is of course also reflected in the experimental data.[24–27,29,30] From the comparison in Fig. 4 to the experimental results in Ref. 29, which still seem to be the only ones obtained at low temperatures, one can see that in fact the calculated real part of $\varepsilon(\omega) = [2\varepsilon_{xx}(\omega) + \varepsilon_{zz}(\omega)]/3$ fits rather well to the experimental data, while in the imaginary part, small deviations from the experimental result have to be acknowledged. Possible reasons for these deviations can be (i) an insufficient convergence with respect to the number of substrate layers considered and (ii) the fact that the use of Luttinger's formulation requires to specify a small imaginary frequency δ,[13] here set to 0.653 eV, which
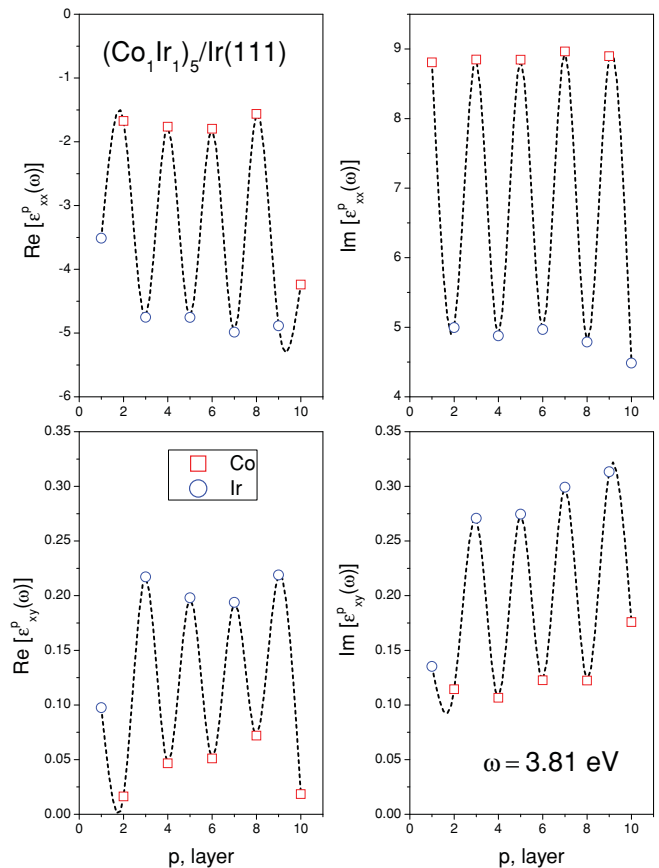

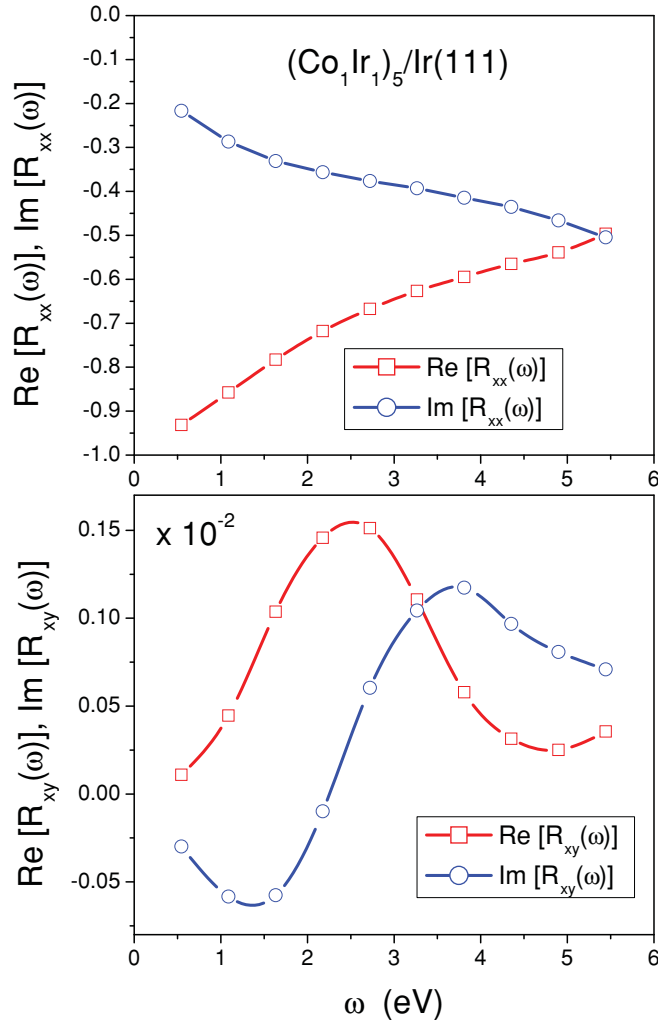FIG. 5. (Color online) Layer-dependent permittivities in $(Co_1Ir_1)_5$/Ir(111) for a frequency of 3.81 eV.

FIG. 6. (Color online) Diagonal and off-diagonal elements of the permittivities for the top Co and Ir layer in $(Co_1Ir_1)/_5Ir(111)$ as a function of frequency.

causes the calculated values below ≈ 1.5 eV to be perhaps less reliable. However, one has to consider also the fact that the experimental data are almost 40 years old and were recorded at a temperature of 77 K while our calculations refer to zero temperature. Altogether, however, the calculated data agree rather well with the experimental ones.

2. Co/Ir superstructure on Ir(111)

In Fig. 5, the real and the imaginary parts of the layer-resolved permittivity-tensor elements $\varepsilon_{xx}^p(\omega)$ and $\varepsilon_{xy}^p(\omega)$ at $\omega = 3.81$ eV are displayed for five repetitions of (Co_1Ir_1) on Ir(111) versus the number of layers p, where $p = 10$ refers to the top Co layer. It is interesting to note that for the diagonal elements of the layer-resolved permittivity tensors the Co layers are dominant, while the off-diagonal elements are dominated by the Ir layers.

The frequency dependence of $\varepsilon_{xx}^p(\omega)$ and $\varepsilon_{xy}^p(\omega)$ with p corresponding to the top Co layer and the Ir layer beneath in $(Co_1Ir_1)_5/Ir(111)$ is shown in Fig. 6. Quite obviously, with the exception of the Co-like $\varepsilon_{xy}^p(\omega)$, all other quantities are strongly frequency dependent. The imaginary part of $\varepsilon_{xy}^p(\omega)$
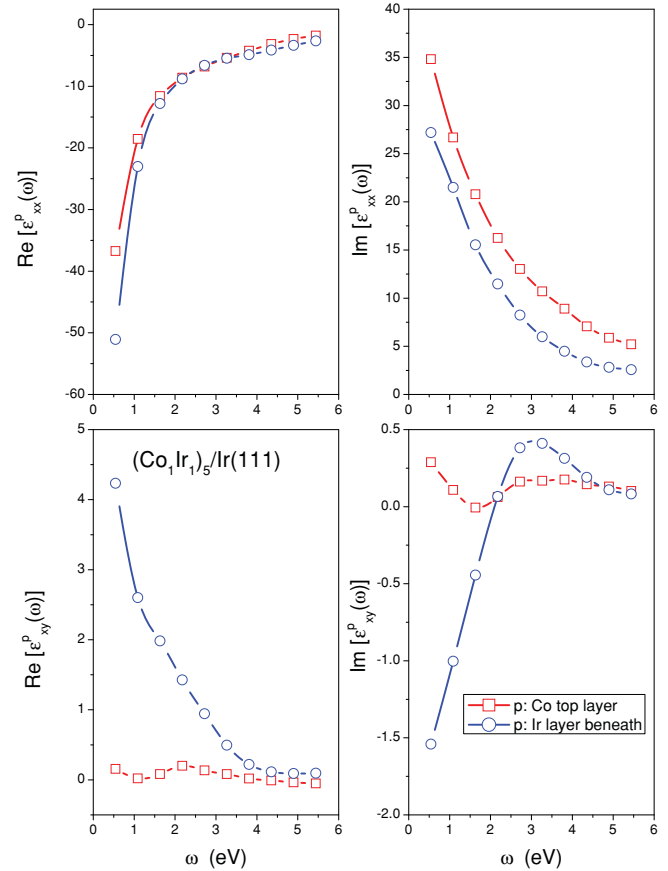

FIG. 7. (Color online) Diagonal and off-diagonal elements of the surface reflectivity matrix in $(Co_1Ir_1)_5/Ir(111)$ as a function of frequency.

for the Ir layer has a maximum at about $\omega = 3.5$ eV, explaining thus the perhaps unexpected size of $Im[\varepsilon_{xy}^p(\omega)]$ for the Ir layers in Fig. 5.

It should be noted that since the $\varepsilon_{xx}^p(\omega)$ and $\varepsilon_{xy}^p(\omega)$ determine the (layer-resolved complex) refraction vectors $n_{pz} = \pm\sqrt{\varepsilon_{xx}^p(\omega) \pm i\varepsilon_{xy}^p(\omega)}$ and $\varepsilon_{xx}^p(\omega) - \varepsilon_{zz}^p(\omega) \sim 0$ (solutions of the Fresnel equation, polar geometry), which in turn enter the Helmholtz equation, $\sum_\nu (n_p^2\delta_{\mu\nu} - n_{p\mu}n_{p\nu} - \epsilon_{\mu\nu}^p)E_{p\nu} = 0, (\mu,\nu = x,y,z)$ and the curl Maxwell equation, $\vec{H}_p = \vec{n}_p \times \vec{E}_p$, for details see Ref. 14, where $\vec{H}_p$ refers to the magnitudes of the magnetic field in layer p and $\vec{E}_p$ is the corresponding electric field, these layer-dependent permittivities govern the optical (macroscopic) part of magneto-optical phenomena. This is particularly important to recall, since the Kerr rotation and ellipticity angles are determined only by the elements of the surface reflectivity matrix in Eqs. (10) and (11).

C. Surface reflectivity matrix

As an example for the surface reflectivity matrix, again, the system $(Co_1Ir_1)_5/Ir(111)$ is chosen. In Fig. 7, the frequency dependence of the real and the imaginary parts of the diagonal and off-diagonal elements of the $\mathbf{R}(\omega)$ are shown for this system. While $Re[R_{xx}(\omega)]$ and $Im[R_{xx}(\omega)]$ increase or decrease almost linearly with ω, $Re[R_{xy}(\omega)]$ and $Im[R_{xy}(\omega)]$ exhibit an oscillatory behavior. In particular, the position of

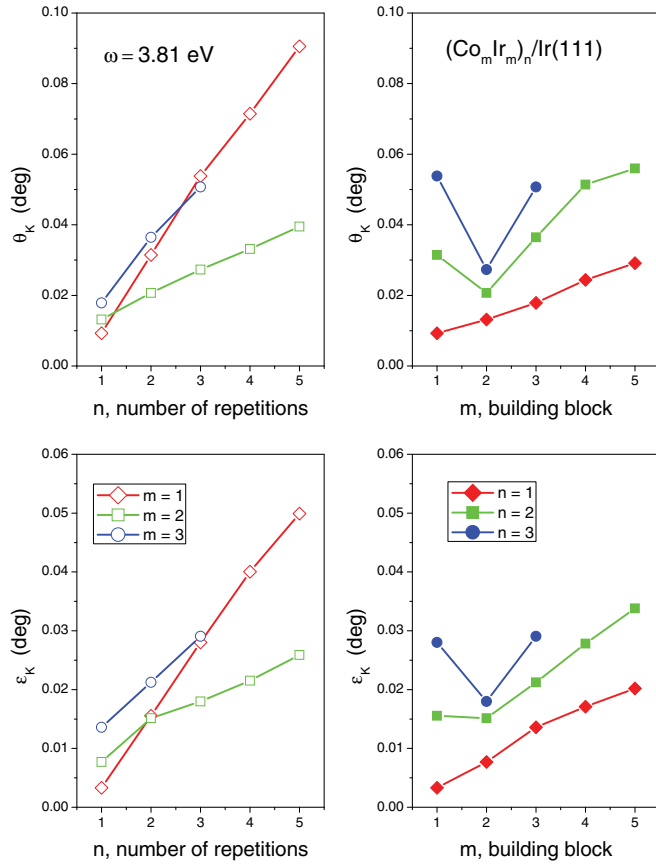FIG. 8. (Color online) Kerr rotation (top) and ellipticity (bottom) angles in $(Co_mIr_m)_n/Ir(111)$ displayed versus n (left panel) and m (right panel).

the maximum in $Im[R_{xy}(\omega)]$ at about 3.8 eV has to be kept in mind for the discussion in the next section.

D. Kerr rotation and ellipticity angles

In Figs. 8 and 9, finally the Kerr rotation $\theta_K(\omega)$ and ellipticity $\varepsilon_K(\omega)$ angles for $(Co_mIr_m)_n/Ir(111)$ are displayed. Figure 8 shows the variation of $\theta_K(\omega)$ (top row) and $\varepsilon_K(\omega)$ (bottom row) at a particular frequency, namely 3.81 eV, with respect to either n (left panel) or m (right panel). It is quite remarkable to observe that independent of the building block (m), $\theta_K(\omega)$ as well as $\varepsilon_K(\omega)$ depend almost linearly on the number of repetitions n, with the exception of $n = 1$; it is not the case when varying the thickness of the Co and Ir layers (m). Only for $m \geqslant 2$ both Kerr angles increase with increasing m.

Because of the linear increase of both Kerr angles with the number of repetitions for each value of m, they are displayed in Fig. 9 normalized by the number of repetitions as a function of frequency. For $m \geqslant 3$, the functional form of $\theta_K(\omega)/n$ and $\varepsilon_K(\omega)/n$ with respect to ω is very similar; at about 3.81 eV, there is a pronounced maximum in $\theta_K(\omega)/n$, while $\varepsilon_K(\omega)/n$ tends to a maximum at high frequencies, $\omega \geqslant 5.5$ eV. At about 2.7 eV, there is a weak minimum in $\varepsilon_K(\omega)/n$. Obviously, the entries for $m = 1$ and 2 are different. For $m = 1$, the maximum in $\theta_K(\omega)/n$ moves toward lower frequencies with increasing n and only for $n \geqslant 2$, the ellipticity
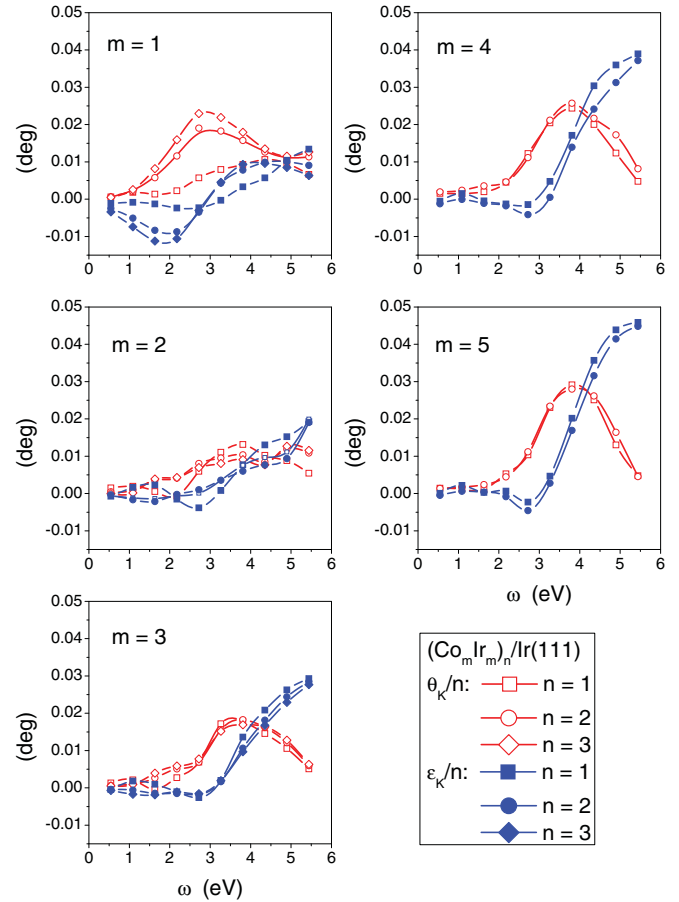

FIG. 9. (Color online) Frequency-dependent Kerr rotation θ_K and ellipticity ϵ_K angles normalized to the number of repetitions (n) in $(Co_mIr_m)_n/Ir(111)$ and represented as a function of frequency.

angle $\varepsilon_K(\omega)/n$ starts to assume the same functional form with respect to ω as for $m \geqslant 3$. The frequency dependence for $m = 2$ seems to be an exception as compared to all other cases, since the values of $\theta_K(\omega)/n$ decrease slightly with n and both $\theta_K(\omega)/n$ and $\varepsilon_K(\omega)/n$ are somewhat smaller than in the other cases. The reason for this strange behavior might very well be the type of coupling between the two Co layers, namely that for an fcc stacking, an interlayer spacing is corresponding to that of bulk fcc Ir, thus a competition between ferro- and antiferromagnetic coupling between the Co layers occurs in contrast to an exclusively ferromagnetic coupling for $m \geqslant 3$.

The maximum of $\theta_K(\omega)/n$ at about 3.81 eV clearly was the reason of choosing exactly this frequency in Figs. 3, 5, and 8. Comparing now Fig. 9 with Figs. 6 and 7 indicates that this maximum is mainly caused by the imaginary part of the off-diagonal element of the surface reflectivity matrix (Fig. 7), which in turn arises from the maximum in the $Im[\varepsilon_{xy}^p(\omega)]$ for the Ir layers (Fig. 6). In short, this maximum has to be attributed to the Ir layers in the $(Co_mIr_m)_n$ superstructures and not to the Co layers.

V. CONCLUSIONS

It was one of the purposes of the present paper to show that although the magneto-optical measurement in terms of

Kerr intensities became a standard procedure in any kind of nanomagnetic investigation, a theoretical interpretation of the underlying magneto-optical constants is by no means straightforward. Also, careful measurements of Kerr rotation and ellipticity angles seem not to be very easy to perform. As has been shown, a theoretical description has to include not only an evaluation of the underlying microscopic quantities, i.e., the optical conductivity tensor, but in addition, has to describe properly also the classical optics part, i.e., the macroscopic part, by taking into account all interferences and reflections.

From the relation in Eq. (15) and from Fig. 9 it follows that, independent of the frequency, for superstructures of the type $(Co_m Ir_m)_n$ on Ir(111), $m \geqslant 3$, the Kerr rotation or ellipticity angles are almost linearly proportional to the total magnetic moment M of the system:

$$\theta_K(\omega) = k_\theta M \sim mn\, k_\theta \langle m_{Co} \rangle,$$
$$\varepsilon_K(\omega) = k_\varepsilon M \sim mn\, k_\varepsilon \langle m_{Co} \rangle.$$

These relations might be important for technical applications.

The frequency dependence of the Kerr rotation angles showed that an optimal frequency can be chosen, namely $\omega \sim 3.8$ eV, at which the $\theta_K(\omega)$ are the largest. Surprisingly enough, this maximum is mainly caused by the Ir "spacer" layers, see Fig. 6. This maximum turned out to be primarily a consequence of the imaginary part of the off-diagonal element of the surface reflectivity matrix and therefore cannot be simply related to the magnetic structure in the Co/Ir superstructures.

*Present address: Uppsala University, Uppsala, Sweden.

[1] J. Kerr, Philos. Mag. **3**, 321 (1877).

[2] J. Kerr, Philos. Mag. **5**, 161 (1878).

[3] P. Weinberger, Philos. Mag. Lett. **88**, 897 (2008).

[4] C. Liu and S. D. Bader, J. Vac. Sci. Technol. A **8**, 2727 (1990).

[5] Z. Q. Qiu, J. Pearson, and S. D. Bader, Phys. Rev. B **45**, 7211 (1992).

[6] E. R. Moog, J. Zak, and S. D. Bader, J. Appl. Phys. **69**, 880 (1991); **69**, 4559 (1991).

[7] X. Gao, D. W. Glenn, S. Heckens, D. W. Thompson, and J. A. Woollam, J. Appl. Phys. **82**, 4225 (1997).

[8] G. Didrichsen, W. R. Hendern, R. Atkinson, R. J. Pollard, and I. W. Salter, J. Magn. Magn Mater. **198**, 558 (1999).

[9] I. Reichl, J. Zabloudil, R. Hammerling, A. Vernes, L. Szunyogh, and P. Weinberger, Phys. Rev. B **73**, 054402 (2006).

[10] Y. Luo, B. Pfeifer, A. Kaeufler, M. Moske, and K. Samwer, J. Appl. Phys. **87**, 2479 (2000).

[11] J. S. Tsay and Y. C. Liu, J. Phys. Condens. Matter **20**, 445003 (2008).

[12] M. Mansuripur, *The principles of Magneto-Optical Recording* (Cambridge University Press, Cambridge, 1995).

[13] L. Szunyogh and P. Weinberger, J. Phys. Condens. Matter **11**, 10451 (1999).

[14] A. Vernes, L. Szunyogh, and P. Weinberger, Phys. Rev. B **65**, 144448 (2002).

[15] A. Vernes, L. Szunyogh, and P. Weinberger, Phys. Rev. B **66**, 214404 (2002).

[16] P. Weinberger, *Magnetic Anisotropies in Nanostructured Matter* (CRC, Boca, Raton, London New York, 2008).

[17] J. Zabloudil, R. Hammerling, L. Szunyogh, and P. Weinberger, *Electron Scattering in Solid Matter* (Springer, Berlin, Heidelberg, New York, 2004).

[18] J. M. Luttinger, in *Mathematical Methods in Solid State and Superfluid Theory*, edited by R. C. Clark and G. H. Derrick (Oliver and Boyd, Edingburgh, 1967) p. 157, Chap. 4.

[19] A. Vernes, L. Szunyogh, and P. Weinberger, J. Phys. Condens. Matter **13**, 1529 (2001).

[20] R. Kubo, J. Phys. Soc. Jpn. **12**, 570 (1957).

[21] S. H. Vosko, L. Wilk, and M. Nusair, Can. J. Phys. **58**, 1200 (1980).

[22] I. Reichl, A. Vernes, C. Sommers, L. Szunyogh, and P. Weinberger, Philos. Mag. **84**, 2543 (2004).

[23] C. Etz, J. Zabloudil, P. Weinberger, and E. Y. Vedmedenko, Phys. Rev. B **77**, 184425 (2008).

[24] J. H. Weaver, Phys. Rev. B **11**, 1416 (1975).

[25] A. Lehmuskero, M. Kuittinen, and P. Vahimaa, Opt. Express **15**, 10744 (2007).

[26] G. P. Hansen, S. Krishan, R. H. Hauge, and J. L. Margrave, Appl. Opt. **28**, 1885 (1989).

[27] G. Haas, G. F. Jacobus, and W. R. Hunter, J. Opt. Soc. **57**, 758 (1967).

[28] Landolt-Börnstein, *Numerical Data and Functional Relationships in Science and Technology, New Series* (1985) Vol. III/15b, p. 372.

[29] M. M. Kirilova, L. V. Nomerovannaya, and M. M. Noskov, Phys. Met. Metallogr. **34**, 61 (1972).

[30] S. Romaine, R. Bruni, P. Gorenstein, and Z. Zhong, Appl. Opt. **46**, 185 (2007).